

Two generations of exsolution lamellae in pyroxene from Asuka 09545: Clues to the thermal evolution of silicates in mesosiderite

LIDIA PITTARELLO^{1,*}, SEANN MCKIBBIN^{1,†}, AKIRA YAMAGUCHI², GANG JI^{3,‡},
DOMINIQUE SCHRYVERS³, VINCIANE DEBAILLE⁴, AND PHILIPPE CLAEYS¹

¹Analytical, Environmental, and Geo-Chemistry (AMGC), Vrije Universiteit Brussel, Pleinlaan 2, B-1050 Brussels, Belgium

²National Institute of Polar Research, Antarctic Meteorite Research Center, 10-3 Midoricho, Tachikawa, Japan

³Electron Microscopy for Materials Science (EMAT), University of Antwerp, Groenenborgerlaan 171, B-2020 Antwerp, Belgium

⁴Laboratoire G-Time (Géochimie: Traçage isotopique, minéralogique et élémentaire), Université Libre de Bruxelles, Av. F.D. Roosevelt 50, 1050 Brussels, Belgium B-1050 Brussels, Belgium

ABSTRACT

Mesosiderite meteorites consist of a mixture of crustal basaltic or gabbroic material and metal. Their formation process is still debated due to their unexpected combination of crust and core materials, possibly derived from the same planetesimal parent body, and lacking an intervening mantle component. Mesosiderites have experienced an extremely slow cooling rate from ca. 550 °C, as recorded in the metal (0.25–0.5 °C/Ma). Here we present a detailed investigation of exsolution features in pyroxene from the Antarctic mesosiderite Asuka (A) 09545. Geothermobarometry calculations, lattice parameters, lamellae orientation, and the presence of clinoenstatite as the host were used in an attempt to constrain the evolution of pyroxene from 1150 to 570 °C and the formation of two generations of exsolution lamellae. After pigeonite crystallization at ca. 1150 °C, the first exsolution process generated the thick augite lamellae along (100) in the temperature interval 1000–900 °C. By further cooling, a second order of exsolution lamellae formed within augite along (001), consisting of monoclinic low-Ca pyroxene, equilibrated in the temperature range 900–800 °C. The last process, occurring in the 600–500 °C temperature range, was likely the inversion of high to low pigeonite in the host crystal, lacking evidence for nucleation of orthopyroxene.

The formation of two generations of exsolution lamellae, as well as of likely metastable pigeonite, suggest non-equilibrium conditions. Cooling was sufficiently slow to allow the formation of the lamellae, their preservation, and the transition from high to low pigeonite. In addition, the preservation of such fine-grained lamellae limits long-lasting, impact reheating to a peak temperature lower than 570 °C. These features, including the presence of monoclinic low-Ca pyroxene as the host, are reported in only a few mesosiderites. This suggests a possibly different origin and thermal history from most mesosiderites and that the crystallography (i.e., space group) of low-Ca pyroxene could be used as parameter to distinguish mesosiderite populations based on their cooling history.

Keywords: Pyroxene, exsolution, mesosiderite, thermal history, cooling rate

INTRODUCTION

Mesosiderites are stony-iron meteorites that consist of a breccia containing roughly equal amounts of metal and silicate (e.g., Prior 1918; Rubin and Mittlefehldt 1993). The metal component shows some similarities to IIIAB iron meteorites (Hassanzadeh, et al. 1990), whereas the silicate fraction has been compared with basaltic or pyroxenitic Howardite-Eucrite-Diogenite (HED) meteorites (e.g., Clayton and Mayeda 1996; Greenwood et al. 2015). A common origin of the silicate fraction of mesosiderites and the HED from the asteroid 4-Vesta has been disproved (Rubin and Mittlefehldt 1993) and recently proposed again (Haba et al. 2019). The simultaneous presence of silicate and metal is interpreted as

a mixture of basaltic material from the crust and metal from the core, originating either by collision of two differentiated parent bodies (Wasson and Rubin 1985) or from mixing within the same parent body (Mittlefehldt et al. 1998; Scott et al. 2001). The silicate fraction generally consists of basaltic to cumulate gabbro and pyroxenitic clasts, locally including olivine nodules exhibiting thick reaction rims (e.g., Ruzicka et al. 1994). Mesosiderites are classified on the basis of their internal structure and relative abundance of plagioclase and pyroxene minerals (Powell 1971; Floran 1978). One of the most peculiar characteristics of mesosiderites is that the metal has recorded the slowest cooling rate from ca. 550 °C ever measured in the solar system, recently re-evaluated to 0.5 °C/Ma (e.g., Powell 1969; Kulpecz and Hewins 1978; Haack et al. 1996; Goldstein et al. 2014).

The formation processes of mesosiderites are still debated, and since Prior (1918) several models have been proposed, involving planetary differentiation (Delaney 1983), collision with a metal projectile (Wasson and Rubin 1985), and remelting of mixed basalt-gabbro and metal close to the parent body surface

* Present address: Department of Mineralogy and Petrography, Natural History Museum Vienna, Burggring 7, A-1010 Vienna, Austria. Orcid 0000-0002-1080-0226. E-mail: lidia.pittarello@univie.ac.at

† Present address: Geowissenschaftliches Zentrum, Georg-August Universität, Goldschmidtstraße 1, 37073 Göttingen, Germany.

‡ Present address: University of Lille, CNRS, INRA, ENSCL, UMR 8207, UMET, Unité Matériaux et Transformations, F-59000 Lille, France.

(Mittlefehldt 1990). The currently most credited formation model (e.g., Rubin and Mittlefehldt 1993; Scott et al. 2001) hypothesizes accretion, followed by a series of crustal melting phases between 4.56 and 4.47 Ga, collisional disruption and gravitational reassembly (3.9 Ga), and finally impact excavation and ejection of buried material. Mixing of metal and crustal silicate should have occurred during one of the crustal remelting phases. This model provides an explanation for the mixture of crustal and core material and for the slow cooling of metal due to deep burial of the mixed material but still fails to fully explain why no mesosiderites have been found bearing olivine-rich silicate fractions or rapidly cooled metal (Hewins 1983). However, the thermal history of the mesosiderite parent body is well constrained. After the mixing event (ca. 4.4 Ga), likely of cold silicate with molten metal, mesosiderites experienced fast cooling to ~800 °C, deep burial in the regolith, and subsequent slow cooling below 800 °C (Stewart et al. 1994; Haack et al. 1996). A similar history has been constrained by Sm-Nd geochronology (Stewart et al. 1994). The young Ar-Ar ages, which were previously interpreted as an impact-induced resetting at 3.9 Ga (Bogard et al. 1990), might simply be caused by the extremely slow cooling of the mesosiderites through the closure temperature for Ar diffusion (Bogard and Garrison 1998). Haba et al. (2017) dated a younger event in zircon than the common formation age, suggesting that this high-temperature event could be either the age of mixing between metal and silicate or a large collision that reheated the whole body. An internal formation hypothesis was proposed by Delaney (1983), but rejected by later studies (e.g., Hewins 1983). In the Earth, the delivery of subducted oceanic basaltic crust to the core-mantle boundary (van der Hilst and Karason 1999; Andraut et al. 2014) might lend some inspiration to an internal formation process for mesosiderites, through internal convection in planetesimals such as the HED parent body (Tkalcic et al. 2013).

However, there are many differences between the Earth and the possible mesosiderite parent body, and mesosiderites can be explained also by migration of core liquids to the crust via metallic volcanism (e.g., Johnson et al. 2019). A recently proposed formation hypothesis of mesosiderites involves a hit-and-run collision on Vesta and burial under a thick blanket of collisional debris, based on accurate zircon dating (Haba et al. 2019).

The cooling history of the silicate fraction in mesosiderites is not yet clear. Bogard et al. (1990) summarized the three possible scenarios that are consistent with the radiometric ages: after the formation or reheating up to 1150 °C at 4.5 Ga, silicates underwent (1) rapid cooling (1 °C/yr), followed by slow cooling (1 °C/Ma) of the metal, (2) slow cooling, (3) further reheating event at ca. 4 Ga, followed by rapid cooling of silicates down to 550 °C and subsequent slow cooling of the metal. Bogard et al. (1990) proposed a fourth scenario, where metal silicate mixing occurred at 4.5 Ga, but an important reheating event (temperature peak lower than 550 °C) occurred later at <4 Ga. The estimated peak temperature would have been sufficient to reset the Ar age but not to affect the silicates. Most estimates agree that the silicate cooling rate was fast until ca. 800 °C (Delaney 1983; Ruzicka et al. 1994; Ganguly et al. 1994; Stewart et al. 1994), with proposed values of 1–100 °C/day (based on pyroxene overgrowth; Delaney et al. 1981), and 14 °C/ka at 1150 °C, ca. 5 °C/ka at 600 °C, and 1 °C/Ma at 250 °C (based on new data on Fe-Mg diffusion in

pyroxene; Ganguly et al. 1994).

In this work, we present a study of mesosiderite Asuka (A) 09545, collected in Antarctica during a joint Belgian-Japanese mission, focusing on pyroxene to characterize peculiar exsolution processes and constrain the cooling history of silicates in this sample. By comparison with other mesosiderites in the literature, the implications of such observations on the formation processes of mesosiderites are discussed.

METHODS

A polished thin section (thickness 35 mm) and a thick polished chip of sample A 09545 were investigated in this work (Fig. 1a). Scanning electron microscopy (SEM) has been performed at the Royal Belgian Institute of Natural Science (RBINS), Brussels, Belgium, with a FEI Inspect S50 instrument, equipped with an energy-dispersive spectrometry (EDS) detector, and at the Vrije Universiteit Brussel, Brussels, Belgium, with a JEOL 6400 SEM. Experimental conditions were 10 mm of minimum working distance, 15 kV acceleration voltage, ca. 300 pA beam current, and 4–6 mm of spot size. Quantitative analysis of the composition of the investigated phases has been evaluated with a JEOL JXA-8200 electron microprobe, equipped with five wavelength-dispersive spectrometers (WDS) and one EDS, at the National Institute of Polar Research (NIPR), Tachikawa, Japan. Operating conditions were 15 kV acceleration voltage, 12 nA beam current, and with a fully focused beam. Standard ZAF corrections were applied. Detection limits for major elements are: 130 mg/g for Si, 140 mg/g for Ti, 90 mg/g for Al, 170 mg/g for Cr, 230 mg/g for Fe, 240 mg/g for Mn, 60 mg/g for Mg, 60 mg/g for Ca, 110 mg/g for Na, and 100 mg/g for K. Natural and synthetic materials obtained from C.M. Taylor Company were used as mineral reference materials. The composition of pyroxene is expressed as end-member components: enstatite (En) mol%, ferrosilite (Fs) mol%, and wollastonite (Wo) mol%. Image analysis for quantitative petrography has been applied on BSE-SEM images, using the free software ImageJ.

A FEI Helios NanoLab 650 dual beam system (Field Emission-FE-SEM and focused ion beam-FIB) was used to prepare site-specific transmission electron microscopy (TEM) samples by Ga⁺ ion sputtering, with an ion beam accelerating voltage of 30 kV and a beam current of 3 nA. TEM has been performed with a Philips CM20 instrument, operated at 200 kV and equipped with a Nanomegas “Spinning Star” precession unit and an Oxford INCA x-sight EDS detector. Microdiffraction, i.e., with a nearly parallel incident beam focused on the specimen with a spot size in the range 10–50 nm, was performed to acquire a single-crystal zone-axis pattern (ZAP). The precession semi-angle was set to 2° to significantly reduce overall dynamical effects. Java electron microscopy simulator (JEMS) software was used for simulation of electron diffraction patterns assuming a kinematic approximation (Stadelmann 2004). Both instruments are located at the Electron Microscopy for Materials Science (EMAT) laboratory of the University of Antwerp, Belgium. Additional optical microscopy was performed at the Natural History Museum of Vienna, Austria, on selected thin sections of mesosiderites from the local collection.

RESULTS

Petrographic, geochemical, and crystallographic observations

The sections obtained from A 09545 consist of a clast-supported breccia, with gabbroic clasts of various sizes, containing pyroxene and plagioclase, and amoeboid metal (Fig. 1). The metal fraction is 20–30% in volume, as calculated by image analysis on BSE-SEM images. The sample is crosscut by veins with products of alteration and oxidation, due to terrestrial weathering. No olivine has been detected in this fragment. However, a large nodule with an olivine core and a coronal mantle detached from the sample during preparation and was included in the polished chip. In this work, this nodule will not be considered. Plagioclase is anorthitic (An₉₁) and has a homogeneous composition throughout the sample. Silicate clasts contain also chromite, apatite, and a minor amount of free silica, the latter mostly localized in the upper corner of the polished chip (Fig. 1).

According to the mineralogic classification of the silicate fraction (Mittlefehldt et al. 1998), the sample belongs to the compositional class B mesosiderites, due to the high amount of low-Ca pyroxene with respect to plagioclase, ca. 75 to 25%, respectively, as determined by image analysis on BSE-SEM images (class A is more “basaltic” rather than “pyroxenitic” with near equal proportions of plagioclase and pyroxene). The lack of clastic matrix suggests complete recrystallization, a relatively high metamorphic grade, and textural classification of type 3 (Powell 1971; Floran 1978). Overall this sample can be considered a cumulate gabbro (Rubin and Mittlefehldt 1992).

Pyroxene in the clasts can reach several hundreds of micrometers in size. All pyroxene crystals, regardless of their size, contain two generations of exsolution lamellae. The pyroxene host

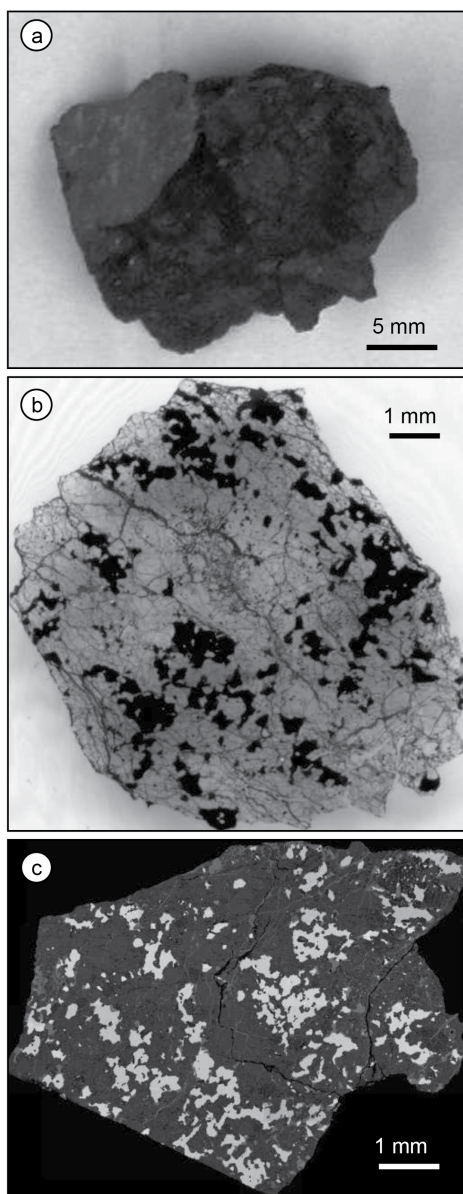


FIGURE 1. Mesosiderite A 09545. (a) Photo of the original meteorite. (b) Thin section optical photo. (c) BSE-SEM image mosaic.

TABLE 1. Chemical composition of the pyroxene clasts and their lamellae as determined with the electron microprobe and TEM-EDS

wt%	Host Px (avg 15)	lam1 (avg 14)	lam1 (EDS) (avg 2)	lam2 (EDS) (avg 2)	Calculated composition lam1+2	Calculated Px original composition
SiO ₂	53.07(22)	52.56(34)	55	52	52.55	53.03
TiO ₂	0.44(3)	0.71(7)			0.61	0.46
Al ₂ O ₃	0.53(3)	0.97(12)			0.84	0.56
Cr ₂ O ₃	0.30(5)	0.48(4)			0.41	0.31
FeO	23.03(31)	10.37(64)	9	27	12.63	22.20
MnO	0.81(5)	0.48(6)			0.41	0.78
MgO	20.96(16)	14.39(24)	15	21	15.32	20.50
CaO	1.58(20)	20.36(49)	21	bdl	17.51	2.85
Na ₂ O	bdl	0.09(2)			0.08	0.02
K ₂ O	bdl	bdl			bdl	bdl
Total	100.72	100.41			100.37	100.71
Si	1.978	1.960	2.03	1.98	1.964	1.977
Ti	0.012	0.020			0.017	0.013
Al	0.021	0.043			0.037	0.025
Cr	0.009	0.014			0.012	0.009
Fe	0.718	0.323	0.28	0.86	0.395	0.692
Mn	0.026	0.015			0.013	0.025
Mg	1.165	0.800	0.83	1.19	0.853	1.139
Ca	0.063	0.813	0.83		0.701	0.114
Na	0.000	0.007			0.006	0.001
Tot cat	3.994	3.995	3.97	4.02	3.998	3.995
Wo	3	42	43	0	36	6
En	59	41	43	58	43	58
Fs	38	17	14	42	21	36
Mg#	62	71	75	58	68	62

Notes: The composition of the original exsolution lamellae and that of the recombined, bulk pigeonite precursor have been determined by relative percentages using image analysis. Composition is expressed in wt% oxides. Element content has been calculated as molar content. Standard deviation is given in parentheses. Avg = average; bdl = below detection limit.

(host Px) is low-Ca clinopyroxene, with composition $Wo_3En_{59}Fs_{38}$ as determined with the electron microprobe (Table 1), and with a diffraction pattern consistent with monoclinic “ferrosilite” space group $P2_1/c$, which can be technically classified as clinoenstatite considering the chemistry (Fig. 2).

Exsolution lamellae 1 (lam1)

The first generation of exsolution lamellae has an orientation roughly parallel to cleavage and is consistent in all lamellae belonging to the same host grain. Lamellae appear in this section as elongated domains with vermicular shape and lower BSE contrast than the host pyroxene. The average size is 20–30 nm in thickness and up to 100 nm in length, depending on the section. The composition of the lamellae corresponds to augite $Wo_{42}En_{41}Fs_{17}$ (Table 1) and the diffraction pattern to that of monoclinic high-Ca pyroxene (space group $C2/c$; Fig. 2).

Exsolution lamellae 2 (lam2)

Lam1 contains another set of lamellae. Lamellae 2 are organized in subparallel sets, which appear brighter than lam1 in BSE-SEM images. The thickness is generally lower than 300 nm, with a regular spacing of about 900 nm. The composition of lam2 roughly corresponds to $Wo_0En_{56}Fs_{43}$, as determined by standardless EDS-TEM measurements (Table 1), and the diffraction pattern is consistent with that of clinoenstatite (space group $P2_1/c$). The composition and the crystal symmetry, therefore, are similar to those of the host pyroxene, but in lam2 Ca appears to be below the detection limit. The orientation of lam2 has been reestablished to be parallel to [001] (Fig. 3).

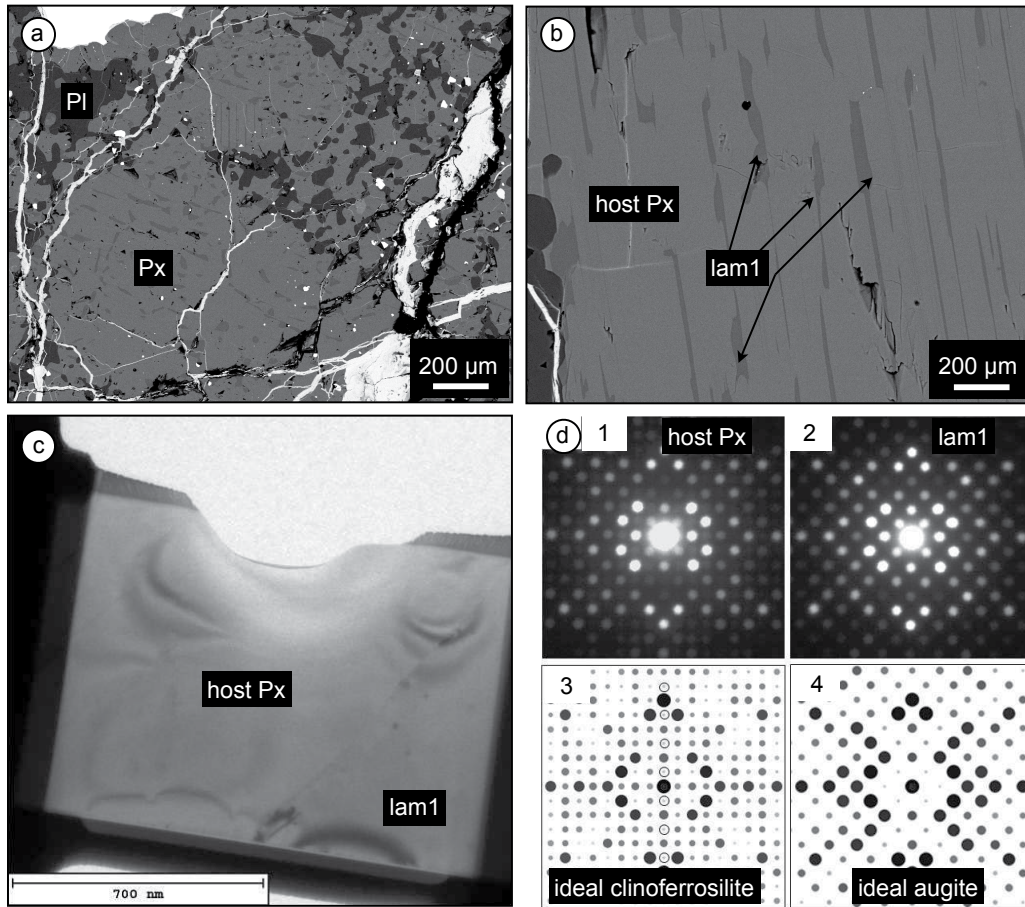


FIGURE 2. First generation of exsolution lamellae in pyroxene from A 09545. (a) BSE-SEM image of the mesosiderite, with gabbroic clasts and interstitial metal. The clasts mostly consist of pyroxene, with augite exsolutions (lam1) with darker BSE contrast than the host low-Ca pyroxene (host Px), and anorthitic plagioclase (PI). (b) Detail of lam1 along cleavage in the low-Ca host. (c) TEM image from the boundary between the host pyroxene (host Px) and augite (lam1). (d) Experimental zone-axis diffraction pattern (ZAP) of host (1) and lam1 (2) and the corresponding simulated $[7\ 0\ 12]$ and $[14\ 0\ 27]$ ZAP, respectively, of clinoferrosilite (3) (similar to that of clinoenstatite) and augite (4).

DISCUSSION

Geothermometric calculations

Equilibration temperatures of the pyroxene phases present in the mesosiderite A 09545 were calculated using the pyroxene geothermobarometers by Lindsley and coworkers (Lindsley 1983, Lindsley and Andersen 1983; Andersen et al. 1993), Brey and Köhler (1990), Putirka (2008), and Nakamuta et al. (2017), as shown in Table 2 and in Figure 4. The graphical and software regression of the pyroxene geothermometer by Lindsley (1983), Lindsley and Andersen (1983), and Andersen et al. (1993) is based on Fe-Mg exchange between augite and a low-Ca pyroxene. The software-aided calculation was performed with QUILF (Andersen et al. 1993), which is unfortunately not supported any longer and required a virtual machine to be run on modern OSs. This geothermometer is completely independent from the pressure and the Ca content in the low-Ca pyroxene, and it considers the presence of pigeonite, rather than orthopyroxene. These characteristics allow the evaluation of the equilibrium temperature for the second generation of exsolution lamellae, even though the Ca content is below the detection limit. A further development, and

improvement, of such a geothermometer was provided by Nakamuta et al. (2017), who considered the influence of minor elements, such as Na, Ti, Mn, Al, Cr, and Na, in the Fs and Wo components to evaluate the crystallization temperature of individual phases. By contrast, Putirka (2008) improved with additional experimental data the geothermometer proposed by Brey and Köhler (1990), which was based on Ca exchange. Additionally, Putirka (2008) included the effect of pressure, calculated from the composition, in an iterative process. As in the investigated A 09545 mesosiderite, the pressure is difficult to evaluate and likely much lower (30–50 MPa) than the experimental range (ca. 1 GPa) of the proposed geothermobarometer (Putirka 2008) and as the Ca content in lam2 is below detection limit, both the geothermometers proposed by Brey and Köhler (1990) and Putirka (2008) do not converge for the second generation of lamellae. In addition, the geothermometer by Putirka (2008) was optimized for Mg# of clinopyroxene >75 and the augite in lam1 in A 09545 has Mg# 71 (Table 1), further calling into question the applicability of such a geothermometer in the investigated mesosiderite.

Table 2 shows the results of the four pyroxene geothermometers selected for this work. As the first exsolution resulted in the augite that

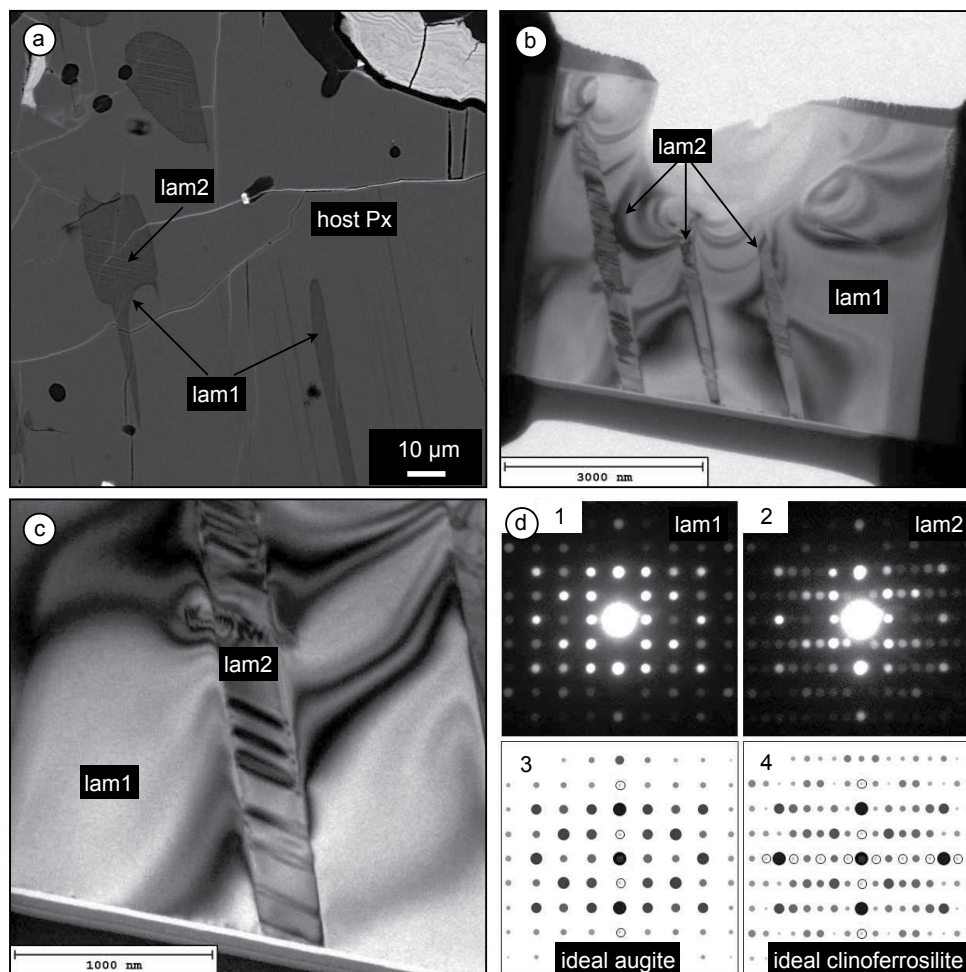


FIGURE 3. Second generation of exsolution lamellae in pyroxene from A 09545. (a) BSE-SEM image of pyroxene, with the augite exsolution lamellae (lam1) with darker BSE contrast and within them lam2 with brighter contrast. (b) TEM image from lam1 with three sub-parallel lam2. (c) Detail from b showing the structural defects within lam2. (d) Experimental ZAP of lam1 (1) and lam2 (2) and the corresponding simulated $[701]$ and $[60\bar{1}]$ ZAP, respectively, of augite (3) and clinoferrosilite (4).

TABLE 2. Comparison of the equilibration temperatures for pyroxene in A 09545, obtained with different geothermometers

	Lindsley et al. 1983 (QUILF)	Brey and Köhler 1990	Putirka 2008	Nakamuta et al. 2017
host – lam1+2	Pgt 907(48) ^{°C}	Opx 994(39) ^{°C}	977 ^{°C}	964–1094 ^{°C}
lam1 – lam2	Pgt 822(32) ^{°C}	Opx 818(86) ^{°C}	834 ^{°C} ^a	323–886 ^{°C}

Notes: Pgt = pigeonite, Opx = orthorhombic pyroxene. Standard deviation is provided in brackets for the geothermometer by Lindsley et al. (1983). The range of temperatures provided according to the geothermometers by Putirka (2008) and Nakamuta et al. (2017) represents the variations obtained adjusting the pressure. See the text for details.

^aWith a pressure of 0.5 kbar and a CaO content in lam2 of 0.01 wt%.

further exsolved low-Ca pyroxene (lam2), the original composition of the augite was calculated by evaluating the contribution of the exsolved lam2 with image analysis (ca. 14% of the surface; Table 1). This calculated composition is called lam1+2 (Table 1). In the geothermometers by Lindsley, Brey and Köhler, and Putirka, the equilibrium was assumed to be between the host low-Ca pyroxene and the lam1+2 augite. The equilibrium conditions between the host and lam1+2 using the geothermometer proposed by Lindsley yields different temperatures, depending on whether the low-Ca pyroxene is considered to be orthopyroxene (994 ± 39 °C) or pigeonite (907 ± 48 °C), regardless of the pressure imposed. The software QUILF

(Andersen et al. 1993) offers the opportunity to leave the composition of one of the two phases as uncertain, to determine the theoretical equilibrium. In this case, the temperature range is from 870 to 1106 °C, depending on the variables. The geothermobarometer of Brey and Köhler (1990) yields a temperature of 977 °C for the first generation of exsolution and that of Putirka (2008) a temperature of 982–1023 °C and a pressure of ca. 2–24 kbar, but with a KD of only 0.75, when it should be close to 1.09 ± 0.14 , suggesting that the two phases were not completely at equilibrium. The obtained temperature with the geothermometer proposed by Nakamuta et al. (2017) is 1094 °C for the lam1+2 composition and 964 °C for the host

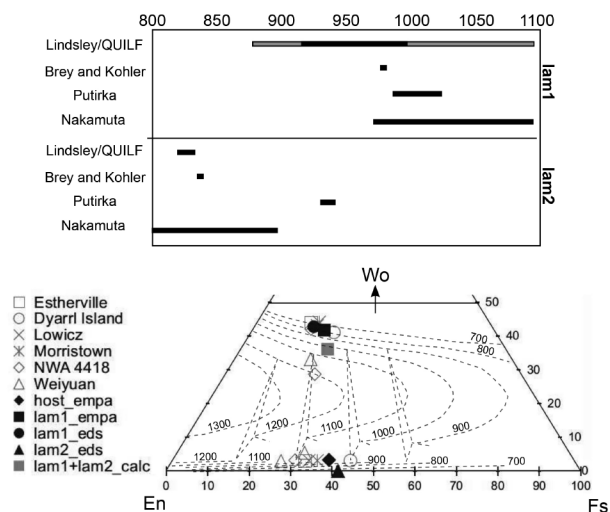


FIGURE 4. Pyroxene composition diagram after Lindsley (1983) and comparison between the geothermometers used in this work for the formation of lam1 and lam2. Data from this work and from literature (Estherville, Lowicz, Morristown, and Dyarr Island after Hewins 1979; Vaca Muerta and Patwar after Mittlefehldt et al. 1998). Note that the host pyroxene and the lam1 plot in a temperature range 800–1000 °C, whereas lam2 seem to be consistent with a low temperature (<500 °C). The geothermometers are abbreviated with the name of the first author or authors and are Lindsley (1983), Lindsley and Andersen (1983), Andersen et al. (1993), Brey and Köhler (1990), Putirka (2008), and Nakamuta et al. (2017). There is a fairly good agreement of all geothermometers for the first exsolution at ca. 950 °C and a good agreement of three over four geothermometers for the second exsolution at 800–850 °C. Data out of range are not shown.

composition. All the four geothermometers provide similar results for the first exsolution and are roughly consistent with the graphical evaluation based on Lindsley (1983; Fig. 4).

The composition of lam2 could be determined only by EDS at the TEM and no Ca was detected. In Putirka (2008), the equilibrium conditions between lam1 and lam2 strongly depend on the CaO content in lam2. Even assuming a CaO content of 0.1–0.2 wt% (a reasonable detection limit for the instrument), the calculation does not converge, unless a very low pressure (0.5 kbar) is imposed. In this case, the geothermometer provides a temperature of 834 °C using the equations of Brey and Köhler (1990) and 915–928 °C using the equations by Putirka (2008). Increasing the imposed pressure by one order of magnitude, to 5 kbar, the temperature evaluation increases by ca. 10 °C. Following the geothermometer of Nakamuta et al. (2017), the temperature for the second exsolution products is 323 °C for the composition of lam2 (although the calculations are very sensitive to the Ca content), and 886 °C for the composition of lam1. QUILF seems not to be affected by the Ca content in lam2, and the resulting temperature variations for a CaO content from 0 to 0.2 wt% are within error. Considering lam2 as a pigeonite, the equilibrium temperature is 822 ± 32 °C, and considering lam2 as an orthopyroxene is 818 ± 86 °C. The various temperature ranges obtained for these different geothermometers are plotted in Figure 4. In any case, the lower content of CaO in the second generation of exsolution leads to lower equilibrium temperatures than those for the first exsolution, as also suggested by the graphical evaluation based on the diagram provided by Lindsley (1983; Fig. 4).

It was postulated that the applicability of the two-pyroxene geothermometer might be affected by the Ca content in pyroxene (e.g., Bunch and Olsen 1974) and the Fe content in augite. The latter effect has been recently demonstrated to be negligible (Murri et al. 2016). The effects of Na, Cr, and Al in octahedral coordination have been taken into account by Nakamuta et al. (2017), updating the geothermometer of Putirka (2008), and turned out to be negligible in our sample. However, geothermometric calculations based on Fe-Mg exchange in pyroxene might provide the peak temperature, rather than the effective closure temperature, in the case of fast cooling rate (100–1000 °C/ka), due to the relatively slow diffusion rate of these elements in clinopyroxene (e.g., Müller et al. 2013).

Cooling rate evaluation

The cooling rate of pyroxene is generally determined by the fractionation of Fe^{2+} and Mg^{2+} between the sites M1 and M2. This is performed by X-ray diffraction techniques (e.g., Mueller 1967; Ganguly 1982; Stimpfl et al. 2005) and by structure refinement of TEM data obtained with the precession technique (e.g., Palatinus et al. 2015, for orthopyroxene). Neither of the two was applied to A 09545 so far; however the applicability is not only hampered by the analytical limitations, but also by the fact that the closure temperature of the ordering has been found to be ca. 500 °C for orthopyroxene (e.g., Ganguly et al. 2013). Thus the calculated cooling rates would correspond to temperatures below those of exsolution and would be equivalent to those evaluated for metallographic exsolution in mesosiderite, for which the cooling rates are already known.

An alternative, although controversial method to evaluate the cooling rate of pyroxene is based on the thickness of exsolution lamellae, assuming that their growth is controlled by the cooling rate. Miyamoto and Takeda (1977) determined the cooling rate of eucrites based on the thickness of pyroxene exsolution lamellae. Extrapolating their evaluation to our sample, we obtain a cooling rate of ca. 1 °C/ka for lam1 and 10 °C/yr for lam2, thus consistent with those proposed by previous studies on mesosiderites (e.g., Ganguly et al. 1994). However, we present these as only very cautious, approximate values. The thickness of lamellae alone has proven not to be reliable in estimating the cooling rate of pyroxene, because it is potentially controlled also by other factors and different lamellae thicknesses can be exhibited in the same sample (e.g., Miyamoto et al. 2001; Sugiura and Kimura 2015).

Additional temperature evaluations based on crystallographic characteristics

The formation of exsolution lamellae at different temperatures has also been related to the angle between the growth direction [considered (001) and (100)] and the *c*-axis of the host (Robinson et al. 1977). This angle decreases for increasing temperature of formation in the range 850–1050 °C. We did not determine the angle between the lattice directions, nor the lattice parameters in A 09545. However, the described features and the lamellae orientation presented by Robinson et al. (1977) match the observations on lam2 in A 09545. In detail, the deformation features observed in lam2 (Fig. 3) might have been caused by the speed in changing symmetry class (from $C2/c$ to $P2_1/c$) that induces lattice strain. The presence of these features and the occurrence of monoclinic, low-Ca pyroxene are consistent with the formation of lam2 at temperatures in the range 750–900 °C, supporting the temperature evaluation provided by the Lindsley geothermometer.

Nakazawa and Hafner (1977) investigated two generations of exsolution lamellae in pyroxene from a Lunar basalt. These authors observed that the crystallographic orientation of lamellae is determined by the crystal symmetry of the original host: lamella along (001) exsolved from $C2/c$ (high pigeonite) and lamellae along (100) derived from $P2_1/c$ pyroxene. The change in the plane of intergrowth depends on the temperature, and in A 09545, the transition between exsolution lamellae subparallel to (100) to those aligned with (001) should have occurred between 550 and 700 °C. However, the initial conditions, such as the composition of the pyroxene involved and the overall cooling in the work by Nakazawa and Hafner (1977) were quite different from those experienced by A 09545, but the presence of (001) lamellae might suggest a similar slow cooling and nucleation from a pigeonite host rather than from orthopyroxene resulting from pigeonite inversion. Grove (1982) used the orientation and the symmetry class of exsolution lamellae in lunar pyroxene to estimate the cooling rate in the temperature range 1100–800 °C. By comparison with the occurrence of exsolution lamellae in A 09545, we roughly obtained a cooling rate of ca. 10 °C/Ma for lam1, and $\gg 0.02$ °C/h for lam2. This would imply a slow cooling rate in the high-temperature range and fast cooling at lower temperature, which is inconsistent with the thermal evolution of mesosiderites, as constrained from the metallographic textures.

The occurrence of monoclinic low-Ca pyroxene as host and in lam2

The occurrence of clinoenstatite, rather than orthoenstatite (latter with space group $Pbca$) as host and in lam2 suggests several possible interpretations. In most instances, where the normal product is a set of augite exsolution lamellae hosted in orthopyroxene, this association would be called pigeonite inversion. It is possible that in some of the previous works on mesosiderites, the identification of orthopyroxene was only based on the low-Ca content, without pursuing further analyses. Even though optical extinction could provide a hint on the crystal symmetry, many samples were not

prepared as petrographic thin sections, and pigeonite with a low $2V$ angle and rounded shape might be difficult to distinguish from orthorhombic pyroxene. According to Ishii and Takeda (1974), exsolution lamellae of augite form along (001) in host metastable pigeonite, whereas augite blebs along (100) form as a result of decomposition of pigeonite into orthopyroxene and augite. The different processes are controlled by the original composition of the pigeonite, which should have been quite Mg-rich to decompose into orthopyroxene and augite, rather than to simply exsolve augite. Although Ishii and Takeda (1974) report the presence in the literature of (100) augite blebs in metastable low-Ca pigeonite (called clinohypersthene) in extraterrestrial material, they do not provide a possible explanation of this apparent contradiction to their analyses. In A 09545, we conclude that it is possible that orthopyroxene did not nucleate at all and that the host, which now consists of metastable pigeonite, was always clinopyroxene, but underwent the transition from $C2/c$ to $P2_1/c$.

Constraining the thermal history of pyroxene from exsolution lamellae

From geothermometric calculations based on the Fe-Mg exchange in pyroxene, together with the other parameters considered in this study (lattice, lamellae orientation, and symmetry inversion/transition), the cooling of pyroxene can be followed step by step from an initial temperature of 1150 °C (crystallization temperature of pigeonite) to ca. 550 °C (inversion of orthopyroxene, if in fact it ever nucleated, into clinopyroxene or alternatively the inversion from high to low pigeonite), as represented in Figure 5.

The cooling rate estimated by Ganguly et al. (1994), based on pyroxene zoning in mesosiderite, yielded 1 °C/100 yr until 850 °C and a progressively lower cooling rate for lower temperatures. A more recent study set the change between the fast and slow cooling rate at approximately 700 °C (Ganguly and Tirone 2001). Our rough calculations indeed suggest a slower cooling rate at high temperature for the formation of lam1, but a faster cooling rate at

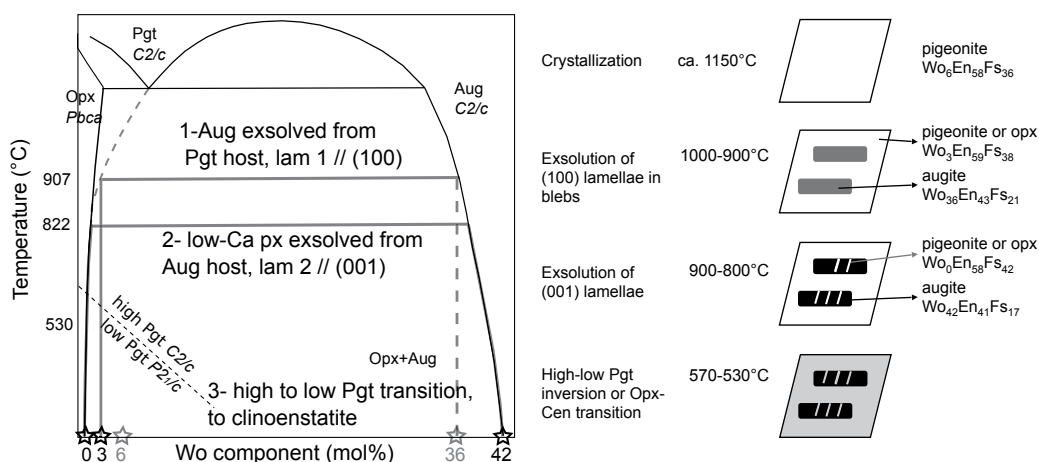


FIGURE 5. Simplified pseudobinary pyroxene phase diagram at low pressure (modified after Lindsley 1983). Composition is expressed as Wo content vs. temperature; with temperature estimates according to QUILF95 (Table 2); and with a schematic representation of the sequence of events affecting the investigated pyroxene in A 09545. Augite (Aug) with a composition of Wo_{36} was exsolved from a host metastable pigeonite (Pgt), rather than from orthopyroxene, with a final composition of Wo_3 . From Aug Wo_{36} , a further exsolution event generated low-Ca px (Wo_0) while the sample was still at relatively high temperature (< 820 °C) and the composition of Aug evolved to Wo_{42} . Finally, the original Pgt underwent transition from high to low Pgt (ca. 530 °C; e.g., Brown et al. 1972). Mineral abbreviations according to Whitney and Evans (2010).

low temperature leading to the formation of lam2.

A definitive evaluation of the cooling rate in the range 700–550 °C would be provided by single-crystal diffraction of the host clinoenstatite and of the first generation lamellae (e.g., Molin et al. 2006), following the method of Stimpfl et al. (2005) and Murri et al. (2016), and by modeling in detail the cation exchange (e.g., McCallum et al. 2006). Unfortunately, the presence of inclusions, the grain size, and the accessibility to crushed samples hamper the applicability of this technique to the investigated mesosiderite A 09545.

Following the current understanding of cation diffusion in pyroxene, numerical modeling has demonstrated that slow heating and slow cooling rates are required for pyroxene to register temperature variation (Yamamoto et al. 2017). This excludes impact reheating as the process to initiate the exsolution in pyroxene because the duration of the process would be too short to reach equilibrium. Rather, it supports the scenario that after initial formation, silicates recorded a single history of cooling and were not reheated above a certain temperature. Even abrupt reheating to above ca. 600 °C, as would be likely during an impact event, would have obliterated the described microstructure.

The cooling path of pyroxene in A 09545 likely involved exsolution of high pigeonite ($C2/c$) hosting augite exsolution lamellae ($C2/c$), followed by high-low pigeonite transformation ($C2/c$ to $P2_1/c$; Tribaudino et al. 2018) as shown in Figure 5. This transition starts at 940 °C in experiments, according to Shimobayashi and Kitamura (1991) and is completed at ~530 °C, according to Brown et al. (1972). Such a metastable transformation skips the orthopyroxene field and enables a restructuring of the host high pigeonite crystal into clinoenstatite with only local rearrangement of the lattice. Another possible path would involve decomposition of pigeonite into orthopyroxene and augite blebs upon slow cooling, followed by a low-temperature transition from orthopyroxene into low-clinopyroxene ($Pbca$ to $P2_1/c$ at 570–600 °C at low pressure; Ulmer and Stalder 2001, and references therein). However, the transformation of the entire host pyroxene from ortho- into clinoenstatite requires complete restructuring of the crystal (Smith 1969; Ashworth 1980) and no unequivocal evidence of the existence of orthopyroxene any time during the sample history is present in the investigated mesosiderite. The failed nucleation of orthopyroxene and the presence of low-Ca pigeonite exsolved from regular pigeonite are not rare in the literature on terrestrial pyroxene (e.g., Bonnichsen 1969; Smith 1974), but were rarely reported in meteorites. This process cannot be exclusively related to the cooling rate, as crystals subjected to the same conditions exhibit variable behavior with regard to the nucleation of orthopyroxene rather than low-Ca pigeonite (e.g., Bonnichsen 1969). The interpretation of a relatively fast cooling rate as necessary to preserve the presence of pigeonite would be in contrast with the hypothesis of relatively slow cooling rate to develop the thick exsolution lam1 and the formation of lam2 from lam1, and with mesosiderite petrogenesis more generally. Nucleation of orthopyroxene in mesosiderites may ultimately be controlled by other characteristics.

Occurrence of exsolution lamellae in pyroxene in other mesosiderite samples

Exsolution lamellae in pyroxene, especially as “inverted pigeonite” (augite in orthopyroxene), have been commonly reported in eucrites and this feature has been interpreted as indicative

of slow cooling after a reheating event >1000 °C (e.g., Yamaguchi et al. 1996). Exsolution lamellae resulting from pigeonite inversion have been described also in a few mesosiderites (e.g., in Alan Hills A77219 by Agosto et al. 1980; in Dyarrl Island, Lowicz, and Patwar by Delaney et al. 1981; in Estherville by Ganguly et al. 1994; in Morristown and Mount Padbury by Powell 1971; and in Vaca Muerta by Rubin and Jerde 1987). However, these have never been investigated in detail. Two generations of exsolution lamellae, similarly to those investigated in this work, were presented by Rubin and Jerde (1987) from the Vaca Muerta mesosiderite. The lithic clasts containing two generations of exsolution lamellae were interpreted by these authors as cumulate eucrite clasts, thermally annealed after incorporation into the mesosiderite. According to Powell (1971), inverted pigeonite with exsolution lamellae along two orientations might be common in the sub-group three mesosiderites, including examples such as Lowicz, Mincy, and Morristown. Our study of A 09545 supports this interpretation. In other mesosiderite sub-groups, inverted pigeonite might be present, but only with exsolution along one direction. That the Vaca Muerta mesosiderite, classified as type 1, contains two orientations of exsolution lamellae in some clasts is consistent with a complex multi-stage history for the petrogenesis of this meteorite. Similarly, in some mesosiderites, the exsolution of inverted pigeonite occurs only at the overgrown rim of orthopyroxene (e.g., in Emery and Morristown; Ruzicka et al. 1994).

Other than data from the literature, additional mesosiderites were investigated, as representative of the variety of mesosiderites, from the collection of the Natural History Museum of Vienna, to search for pyroxene internal features. The most common feature observed in pyroxene in mesosiderites is chemical zoning in low-Ca pyroxene, with a rim enriched in Fe with respect to the core of crystals (e.g., in Estherville, Lamont, and Veramin). This feature is commonly attributed to impact reheating followed by relatively fast cooling and was used to estimate the cooling rate in the range 1150–900 °C as 1–100 °C/day (e.g., Delaney et al. 1981). Inverted pigeonite is relatively common, but two generations of exsolution lamellae, formed at different temperatures during cooling, seems to be rare. However, most of the previous works describe inverted pigeonite as an assemblage of orthopyroxene and augite, without checking by diffraction techniques the real nature of the low-Ca pyroxene. This might actually be clinoenstatite, as in the case of A 09545.

Thermal history of the silicate fraction in the mesosiderite

The silicate fraction of mesosiderites, in particular pyroxene, exhibits a huge variety of internal features. According to Sugiura and Kimura (2015), this variety is due to a range of cooling rates experienced by mesosiderite precursor materials in their parent body after the reheating event. Different burial depths in the parent body might explain these differences. However, this would not be consistent with the model of fast cooling of silicates at high temperature and slow cooling of metal below 700–550 °C. This also excludes the possibility that an important reheating event due to a catastrophic impact could be invoked, with peak temperature <550 °C, because such fine-grained features as the two generations of exsolution lamellae in pyroxene observed in A 09545 would have been completely annealed and obliterated. In conclusion, the variety of microstructures exhibited by mesosiderites indicates

a complex thermal history that cannot be accommodated by a unique model applicable to the whole collection of mesosiderites. However, our study indicates that microstructural investigations may be able to identify internally consistent subgroups within this class of meteorites using pyroxene crystallography in combination with conventional microprobe chemical compositions.

IMPLICATIONS

The internal features of a mesosiderite, investigated by a classical mineralogical approach, provides important new clues to the thermal history of this sample and the evolution of the mesosiderite parent body(ies). In A 09545, clinopyroxene instead of the expected orthopyroxene was found as a host for two generations of exsolution lamellae, suggesting that this sample contains a metastable silicate aggregate. Therefore, the precise characterization of pyroxene crystallography provides additional hints on the cooling rate experienced by the material. Among the numerous open questions about mesosiderite formation, the information on the thermal history of its silicate fraction helps constraining several events that affected this class of meteorites.

The mesosiderite A 09545 (Yamaguchi et al. 2014) contains coarse-grained low-Ca monoclinic pyroxene that hosts two generations of exsolution lamellae, which might shed light on the thermal evolution of the silicate fraction in the sample. Although the exact cooling rate could not be evaluated, the composition, orientation, and lattice parameters of these lamellae provide hints on the thermal evolution of the investigated sample (Fig. 5). We propose a thermal history comprising: (1) formation of the first generation of augite exsolution by cooling through 1000–900 °C; (2) the further exsolution of monoclinic low-Ca pyroxene within augite at 900–800 °C; and (3) at lower temperature, final transformation from high to low pigeonite in the host and in the second generation of exsolution lamellae. By comparison with similar occurrences of exsolution features in pyroxene reported in the literature, we suggest relatively slow cooling in the 900–800 °C range. However, the presence of these features and the unexpected monoclinic crystallography of the low-Ca pyroxene host also imply incomplete equilibrium. Under such conditions, orthopyroxene could likely not nucleate and low-Ca pigeonite has formed instead. Both the two generations of exsolution lamellae and the occurrence of host monoclinic low-Ca pyroxene are uncommon in mesosiderites. The preservation of the investigated exsolution lamellae in pyroxene from mesosiderite A 09545 suggests, for this sample, either a burial depth sufficient to guarantee a relatively slow cooling rate or a reheating event due to impact with a peak temperature lower than 570 °C and, if higher, for a very short duration. The simultaneous occurrence of the above described features in pyroxene points to the possibility that crystallographic investigations could define new mesosiderite subgroups and ultimately new constraints on the thermal history and origin of the mesosiderite parent body.

ACKNOWLEDGMENTS

The samples have been kindly provided by the National Institute of Polar Research, Tachikawa, Japan; the Royal Belgian Institute of Natural Sciences, Brussels, Belgium, and the Natural History Museum Vienna, Austria. The authors thank S. Van Den Broeck for the FIB cut at EMAT, Antwerp, Belgium, and F. Nestola, M. Alvaro, and M. Murri for insightful discussions on the topic. The editor Steven Simon, Donald H. Lindsley and an anonymous reviewer are thanked for insightful comments that greatly improved the manuscript.

FUNDING

This research was funded by the BELAM project and the Interuniversity Attraction Poles Program Planet Topers, both financed by the Belgian Science Policy Office (BELSPO). L.P. is currently funded by the Austrian Science Fund (FWF). S.Mc.K. was supported by a Research Foundation–Flanders (FWO) postdoctoral fellowship (project 1209515N) and is currently a postdoctoral fellow of the Alexander von Humboldt Foundation (project: Early Solar System Pyroxenites). G.J. was supported by the FWO project G.0603.10N.

REFERENCES CITED

- Agosto, W.N., Hewin, R.H., and Clarke, R.S. Jr. (1980) Allan Hills A77219, the first Antarctic mesosiderite. *Geochimica et Cosmochimica Acta*, 44, 1027–1045.
- Andersen, D.J., Lindsley, D.H., and Davidson, P.M. (1993) QUILF: A Pascal program to assess equilibria among Fe-Mg-Mn-Ti oxides, pyroxenes, olivine, and quartz. *Computer & Geosciences*, 9, 1333–1350.
- Andrault, D., Pesce, G., Bouhifd, M.A., Bolfan-Casanova, N., Hénot, J.M., and Mezouar, M. (2014) Melting of subducted basalt at the core-mantle boundary. *Science*, 344, 892–895.
- Ashworth, J.R. (1980) Chondrite thermal histories: Clues from electron microscopy of orthopyroxene. *Earth and Planetary Science Letters*, 46, 167–177.
- Bogard, D.D., and Garrison, D.H. (1998) ³⁹Ar-⁴⁰Ar ages and thermal history of mesosiderites. *Geochimica et Cosmochimica Acta*, 62, 1459–1468.
- Bogard, D.D., Garrison, D.H., Jordan, J.L., and Mittlefehldt, D. (1990) ³⁹Ar-⁴⁰Ar dating of mesosiderites: Evidence for major parent body disruption < 4 Ga ago. *Geochimica et Cosmochimica Acta*, 54, 2549–2564.
- Bonnichsen, B. (1969) Metamorphic pyroxenes and amphiboles in the Biwabik Iron Formation, Dunka river area, Minnesota. *Mineralogical Society of America, Special Paper*, 2, 217–239.
- Brey, G.P., and Köhler, T. (1990) Geothermobarometry in four-phase lherzolites II. New thermobarometers, and practical assessment of existing thermobarometers. *Journal of Petrology*, 31, 1353–1378.
- Brown, G.E., Prewitt, C.T., Papike, J.J., and Sueno, S. (1972) A comparison of the structures of low and high pigeonite. *Journal of Geophysical Research*, 77, 5778–5789.
- Bunch, T.E., and Olsen, E. (1974) Restudy of pyroxene-pyroxene equilibration temperatures for ordinary chondrite meteorites. *Contributions to Mineralogy and Petrology*, 43, 83–90.
- Clayton, R.N., and Mayeda, T.K. (1996) Oxygen isotope studies of achondrites. *Geochimica et Cosmochimica Acta*, 60, 1999–2017.
- Delaney, J.S. (1983) The formation of mesosiderites, pallasites, and other metal-silicate assemblages: two mechanisms. *Meteoritics*, 18, 289–290.
- Delaney, J.S., Nehru, C.S., Prinz, M., and Harlow, G.E. (1981) Metamorphism in mesosiderites. *Proceedings of the 12th Lunar and Planetary Science Conference*, 1315–1342.
- Floran, R.J. (1978) Silicate petrography, classification, and origin of the mesosiderites: review and new observations. *Proceedings of the 9th Lunar and Planetary Science Conference*, p. 1053–1081.
- Ganguly, J. (1982) Mg-Fe order-disorder in ferromagnesian silicates. II. Thermodynamics, kinetics and geological applications. In S.K. Saxena, Ed., *Advances in Physical Geochemistry*, 2, pp. 58–99. *Advances in Physical Geochemistry*, Springer-Verlag.
- Ganguly, J., and Tirone, M. (2001) Relationship between cooling rate and cooling age of mineral: theory and applications to meteorites. *Meteoritics and Planetary Science*, 36, 167–175.
- Ganguly, J., Yang, H., and Ghose, S. (1994) Thermal history of mesosiderites: Quantitative constraints from compositional zoning and Fe-Mg ordering in orthopyroxenes. *Geochimica et Cosmochimica Acta*, 58, 2711–2723.
- Ganguly, J., Tirone, M., Chakraborty, S., and Domanik, K. (2013) H-chondrite parent asteroid: a multistage cooling, fragmentation and re-accretion history constrained by thermometric studies, diffusion kinetic modeling and geochronological data. *Geochimica et Cosmochimica Acta*, 105, 206–220.
- Goldstein, J.I., Yang, J., and Scott, E.R.D. (2014) Determining cooling rates of iron and stony-iron meteorites from measurements of Ni and Co at kamacite-taenite interfaces. *Geochimica et Cosmochimica Acta*, 140, 297–320.
- Greenwood, R.C., Barrat, J.-A., Scott, E.R.D., Haack, H., Buchanan, P.C., Franchi, I.A., Yamaguchi, A., Johnson, D., Bevan, A.W.R., and Burbine, T.H. (2015) Geochemistry and oxygen isotope composition of main-group pallasites and olivine-rich clasts in mesosiderites: implications for the “Great Dunité Shortage” and HED-mesosiderite connection. *Geochimica et Cosmochimica Acta*, 169, 115–136.
- Grove, T.L. (1982) Use of exsolution lamellae in lunar clinopyroxenes as cooling rate speedometers: an experimental calibration. *American Mineralogist*, 67, 251–268.
- Haack, H., Scott, E.R.D., and Rasmussen, K. (1996) Thermal and shock history of mesosiderites and their large parent asteroid. *Geochimica et Cosmochimica Acta*, 60, 2609–2619.
- Haba, M.K., Yamaguchi, A., Kagi, H., Nagao, K., and Hidaka, H. (2017) Trace element composition and U-Pb age of zircons from Estherville: Constraints on the timing of the metal-silicate mixing event on the mesosiderite parent body. *Geochimica et Cosmochimica Acta*, 215, 76–91.
- Haba, M.K., Wotzlaw, J.-F., Lai, Y.-J., Yamaguchi, A., and Schönbächler, M. (2019) Mesosiderite formation on asteroid 4 Vesta by a hit-and-run collision. *Nature*

- Geoscience, 12, 510–515. doi:10.1038/s41561-019-0377-8.
- Hassanzadeh, J., Rubin, A.E., and Wasson, J.T. (1990) Compositions of large metal nodules in mesosiderites: links to iron meteorite group IIIAB and the origin of mesosiderite subgroups. *Geochimica et Cosmochimica Acta*, 54, 3197–3208.
- Hewins, R.H. (1979) The pyroxene chemistry of four mesosiderites. Proceedings of the 10th Lunar and Planetary Science Conference, 1109–1125.
- (1983) Impact versus internal origins for mesosiderites. Proceedings of the 14th Lunar and Planetary Conference. *Journal of Geophysical Research*, 88, B257–B266.
- Ishii, T., and Takeda, H. (1974) Inversion, decomposition and exsolution phenomena of terrestrial and extraterrestrial pigeonites. *Memoirs of the Geological Society of Japan*, 11, 19–36.
- Johnson, B.C., Sori, M.M., and Evans, A.J. (2019) Ferrovolcanism, pallasites, and Psyche. Proceedings of the 50th Lunar and Planetary Science Conference, 1625.
- Kulpecz, A.A. Jr., and Hewins, R.H. (1978) Cooling history of lunar Mg-suite gabbro-norite 76255, troctolite 76535 and Stillwater pyroxenite SC-936: The record in exsolution and ordering in pyroxenes. *Geochimica et Cosmochimica Acta*, 70, 6068–6078.
- Miyamoto, M., and Takeda, H. (1977) Evaluation of a crust model of eucrites from the width of exsolved pyroxene. *Geochemical Journal*, 11, 161–169.
- Miyamoto, M., Mikouchi, T., and Kaneda, K. (2001) Thermal history of the Ibitira noncumulate eucrite as inferred from pyroxene exsolution lamella: Evidence for reheating and rapid cooling. *Meteoritics and Planetary Science*, 36, 231–237.
- Mittlefehldt, D.W. (1990) Petrogenesis of mesosiderites: I. Origin of mafic lithologies and comparison with basaltic achondrites. *Geochimica et Cosmochimica Acta*, 54, 1165–1173.
- Mittlefehldt, D.W., McCoy, T.J., Goodrich, C.A., and Kracher, A. (1998) Non-chondritic meteorites from asteroidal bodies. In J.J. Papike Ed., *Planetary Materials*, 36, pp. 4:1–4:195. Reviews of Mineralogy, Mineralogical Society of America, Chantilly, Virginia.
- Molin, G., Domeneghetti, M.C., Salvio, G., Stimpfl, M., and Tribaudino, M. (2006) Antarctic FRO90011 lodranite: Cooling history from pyroxene crystal chemistry and microstructure. *Earth and Planetary Science Letters*, 128, 479–487.
- Mueller, R.F. (1967) Model for order-disorder kinetics in certain quaternary crystals of continuously variable composition. *Journal of Physical Chemistry Solids*, 28, 2239–2243.
- Muir, I.D. (1954) Crystallization of pyroxenes in an iron-rich diabase from Minnesota. *Mineralogical Magazine*, 30, 376–388.
- Müller, T., Dohmen, R., Becker, H.W., ter Heege, J.H., and Chakraborty, S. (2013) Fe-Mg interdiffusion rates in clinopyroxene: experimental data and implications for the Fe-Mg exchange geothermometers. *Contributions to Mineralogy and Petrology*, 166, 1563–1576.
- Murri, M., Scandolo, L., Fioretti, A.M., Nestola, F., Domeneghetti, M.C., and Alvaro, M. (2016) The role of Fe content on the Fe-Mg exchange reaction in augite. *American Mineralogist*, 101, 2747–2750.
- Nakamura, Y., Urata, K., Shibata, Y., and Kuwahara, Y. (2017) Effect of NaCrSi₃O₈ component on Lindsley's pyroxene thermometer: an evaluation based on strongly metamorphosed LL chondrites. *Meteoritics and Planetary Science*, 52, 511–521.
- Nakazawa, H., and Hafner, S.S. (1977) Orientation relationship of augite exsolution lamellae in pigeonite host. *American Mineralogist*, 62, 79–88.
- Palatinus, L., Correa, C.A., Steciuk, G., Jacob, D., Roussel, P., Boullay, P., Klementova, M., Gemmi, M., Kopeček, J., Domeneghetti, M.C., Camara, F., and Petricek, V. (2015) Structure refinement using precession electron diffraction tomography and dynamical diffraction: tests on experimental data. *Acta Crystallographica B*, 71, 740–751.
- Powell, B.N. (1969) Petrology and chemistry of mesosiderites: I. Textures and composition of nickel-iron. *Geochimica et Cosmochimica Acta*, 33, 789–810.
- (1971) Petrology and chemistry of mesosiderites-II: silicate textures and compositions and metal-silicate relationships. *Geochimica et Cosmochimica Acta*, 35, 3–34.
- Prior, G.T. (1918) On the mesosiderite-grahamite group of meteorites: with analyses of Vaca Muerta, Hainholz, Simondium, and Powder Mill Creek. *The Mineralogical Magazine*, 18, 151–172.
- Putirka, K.D. (2008) Thermometers and Barometers for Volcanic Systems. In K. Putirka and F. Tepley, Eds., *Minerals, Inclusions and Volcanic Processes*, 69, p. 61–120. Reviews in Mineralogy and Geochemistry, Mineralogical Society of America, Chantilly, Virginia.
- Robinson, P., Ross, M., Nord, G.L. Jr., Smyth, J.R., and Jaffe, H.W. (1977) Exsolution lamellae in augite and pigeonite: fossil indicators of lattice parameters at high temperature and pressure. *American Mineralogist*, 62, 857–873.
- Rubin, A.E., and Jerde, E.A. (1987) Diverse eucritic pebbles in the Vaca Muerta mesosiderite. *Earth and Planetary Science Letters*, 84, 1–14.
- Rubin, A.E., and Mittlefehldt, D.W. (1992) Classification of mafic clasts from mesosiderites: implications for endogenous igneous processes. *Geochimica et Cosmochimica Acta*, 56, 827–840.
- (1993) Evolutionary history of the mesosiderite asteroid: a chronologic and petrologic synthesis. *Icarus*, 101, 210–212.
- Ruzicka, A., Boynton, W.V., and Ganguly, J. (1994) Olivine coronas, metamorphism, and the thermal history of the Morristown and Emery mesosiderites. *Geochimica et Cosmochimica Acta*, 58, 2725–2741.
- Scott, E.R.D., Haack, H., and Love, S.G. (2001) Formation of mesosiderites by fragmentation and reaccretion of a large differentiated asteroid. *Meteoritics and Planetary Science*, 36, 869–881.
- Shimobayashi, N., and Kitamura, M. (1991) Phase transition in Ca-poor clinopyroxenes. *Physics and Chemistry of Minerals*, 18, 153–160.
- Smith, J.V. (1969) Crystal structure and stability of the MgSiO₃ polymorphs; physical properties and phase relations of Mg-Fe pyroxenes. *Mineralogical Society of America Special Papers*, 2, 3–29.
- (1974) Pyroxene-olivine-quartz assemblages in rocks associated with the Nain Anorthosite Massif, Labrador. *Journal of Petrology*, 15, 58–78.
- Stadelmann, P. (2004) JEMS-EMS Java version, CIME-EPFL, CH-1015 Lausanne. <https://cime.epfl.ch/research/jems> (accessed on January 8, 2019).
- Stewart, B.W., Papanastassiou, D.A., and Wasserburg, G.J. (1994) Sm-Nd chronology and petrogenesis of mesosiderite. *Geochimica et Cosmochimica Acta*, 58, 3487–3509.
- Stimpfl, M., Ganguly, J., and Molin, G. (2005) Kinetics of Fe²⁺-Mg order-disorder in orthopyroxene: experimental studies and applications to cooling rates of rocks. *Contributions to Mineralogy and Petrology*, 150, 319–334.
- Sugiura, N., and Kimura, M. (2015) Reheating and cooling of mesosiderites. Proceedings of the 46th Lunar and Planetary Conference, 1646.
- Tkalec, B.J., Golabek, G.J., and Brenker, F.E. (2013) Solid-state plastic deformation in the dynamic interior of a differentiated asteroid. *Nature Geoscience*, 6, 93–97.
- Tribaudino, M., Mantovani, L., Mezzadri, F., Calestani, G., and Bromiley, G. (2018) The structure of P₂/c (Ca_{0.2}Co_{0.8})CoSi₂O₆ pyroxene and the C₂c-P₂/c phase transition in natural and synthetic Ca-Mg-Fe²⁺ pyroxenes. *Mineralogical Magazine*, 82, 211–228.
- Ulmer, P., and Stalder, R. (2001) The Mg(Fe)SiO₃ orthoenstatite-clinoenstatite transitions at high pressures and temperatures determined by Raman-spectroscopy on quenched samples. *American Mineralogist*, 86, 1267–1274.
- van der Hilst, R.D., and Karason, H. (1999) Compositional heterogeneity in the bottom 1000 km of Earth's mantle: toward a hybrid convection model. *Science*, 283, 1885–1888.
- Whitney, D.L., and Evans, B.W. (2010) Abbreviations for names of rock-forming minerals. *American Mineralogist*, 95, 185–187.
- Wasson, J.T., and Rubin, A.E. (1985) Formation of mesosiderites by low-velocity impacts as a natural consequence of planet formation. *Nature*, 318, 168–170.
- Yamaguchi, A., Taylor, G.J., and Keil, K. (1996) Global crustal metamorphism of the Eucrite parent body. *Icarus*, 124, 97–112.
- Yamaguchi, A., Pittarello, L., Kimura, M., and Kojima, H. (2014) Meteorite Newsletter 23. National Institute of Polar Research, Tokyo, Japan.
- Yamamoto, J., Ishibashi, H., and Nishimura, K. (2017) Cooling rate responsiveness of pyroxene geothermometry. *Geochemical Journal*, 51, 457–467.

MANUSCRIPT RECEIVED FEBRUARY 15, 2019

MANUSCRIPT ACCEPTED JULY 27, 2019

MANUSCRIPT HANDLED BY STEVEN SIMON